Electronic Supplementary Information (ESI) for

Hierarchically Engineered Polymer Composite with High Solar Reflectivity and Selective Thermal Emissivity for Enhanced Radiative Cooling

Hyunho Park, [a] Beom Soo Joo, [a] Gumin Kang,[a] Hyungduk Ko,*[a] and Jin Hong Kim*[a]*

[a] Nanophotonics Research Center, Korea Institute of Science and Technology, Seoul 02792, Republic of Korea

* E-mail: guminkang@kist.re.kr, kohd94@kist.re.kr, jinhong.kim@kist.re.kr

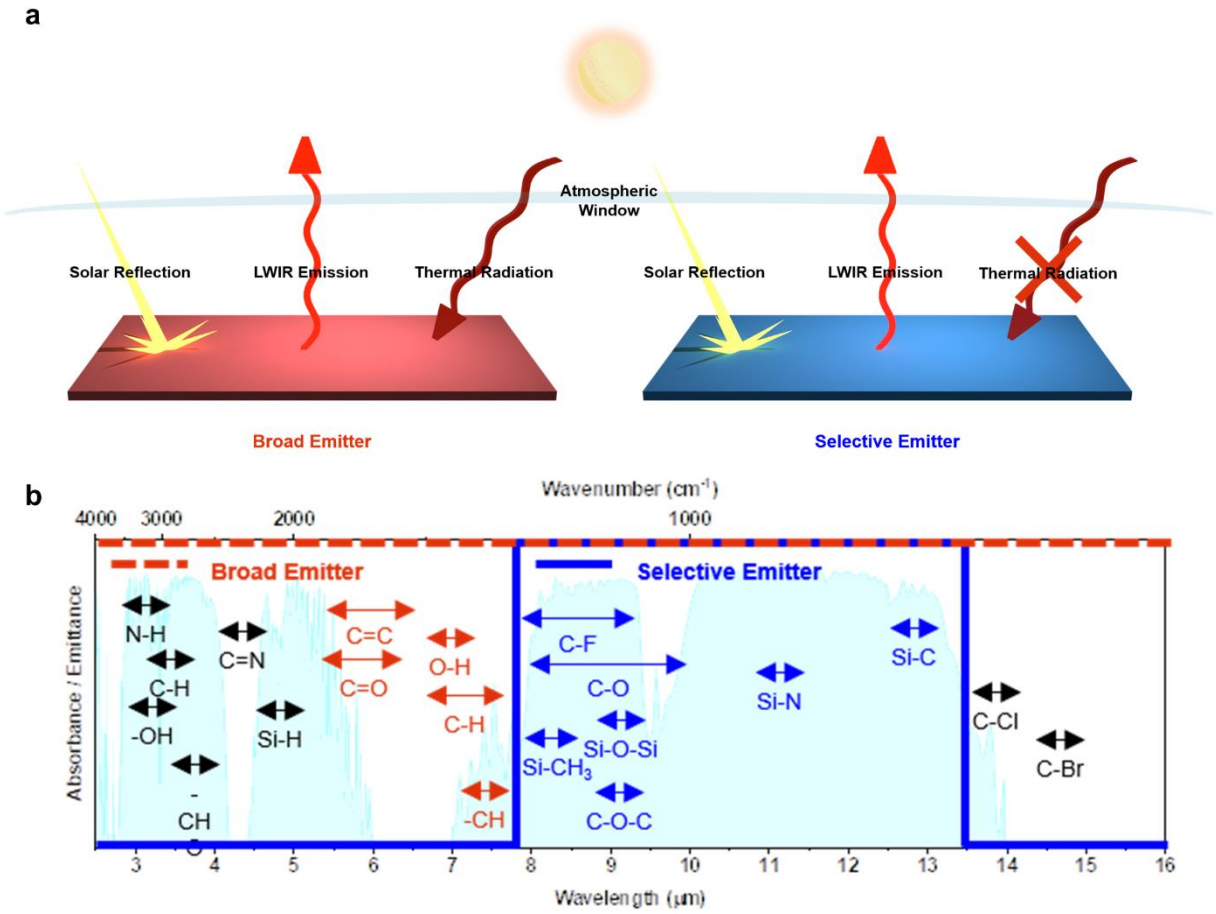

Fig. S1 a) Schematic illustration of the heat transfer processes in a broad emitter and a selective emitter. b) MWIR/LWIR spectra of an ideal broad emitter (red dashed line) and an ideal selective emitter (blue solid line), along with the corresponding major vibrational transition ranges of representative chemical bonds.

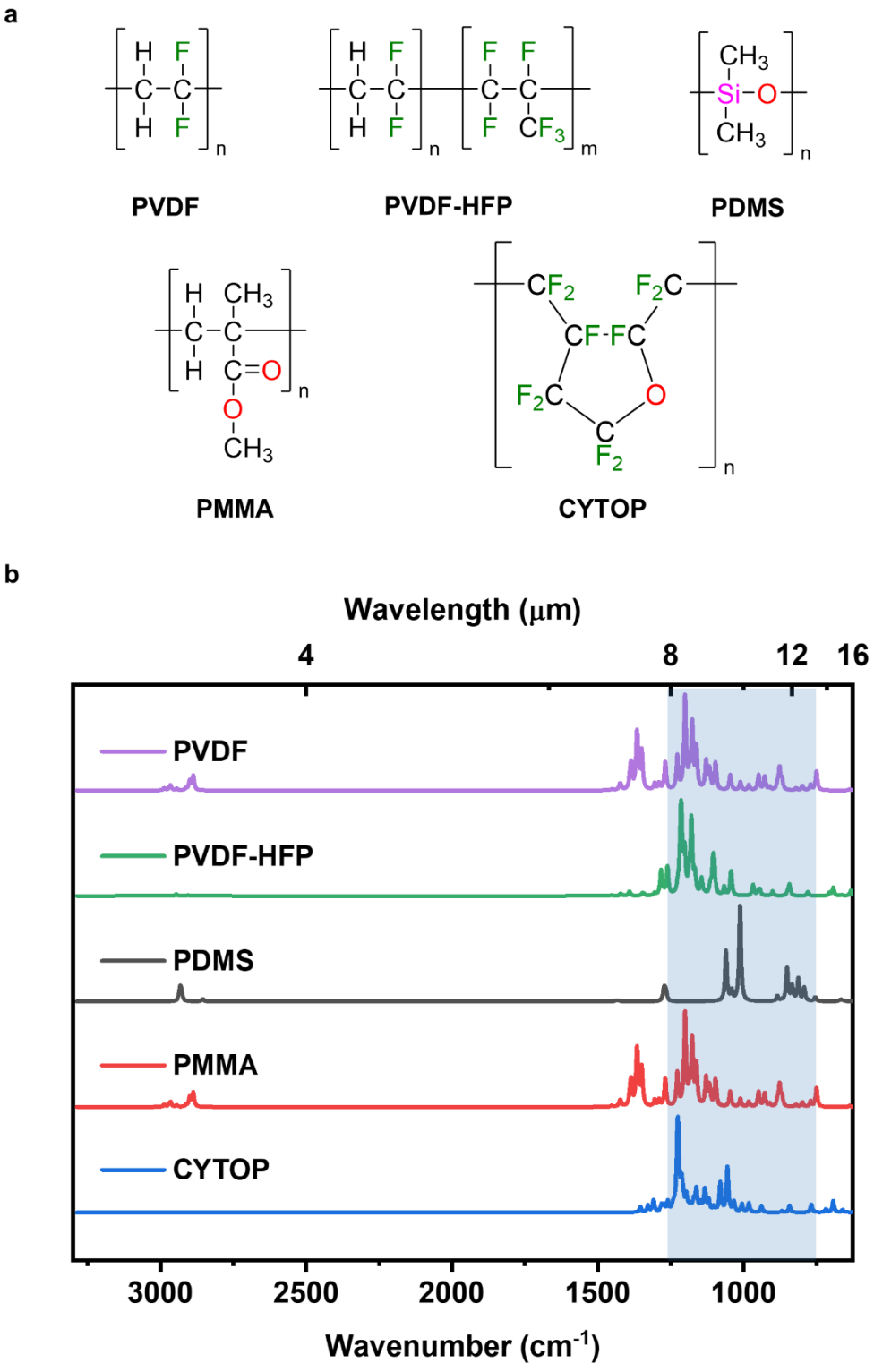

Fig. S2 a) Chemical structures and b) DFT-calculated FTIR spectra of PVDF, PVDF-HFP, PDMS, PMMA, and CYTOP.

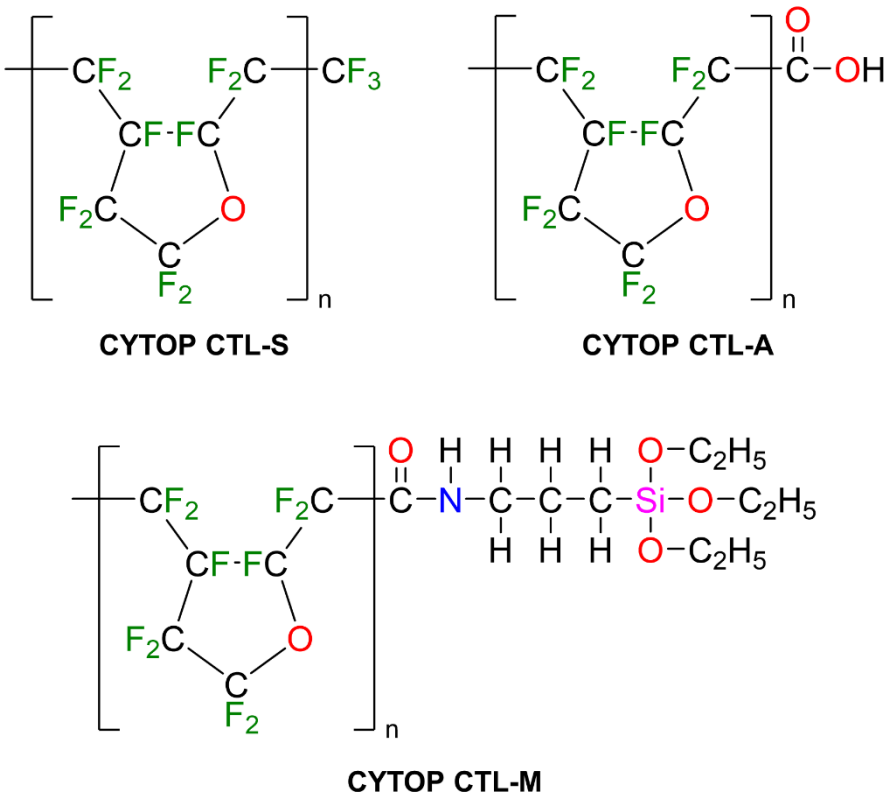

Fig. S3 Chemical structures of various CYTOP models.

Note: Although the main polymer backbone of all CYTOP models consist of C–F and C–O–C chemical bonds, the terminal groups vary, which can affect IR emission. As predicted by DFT theoretical calculations, CYTOP CTL-S is expected to exhibit higher IR selectivity than other models, including CYTOP CTL-M (used in this work).

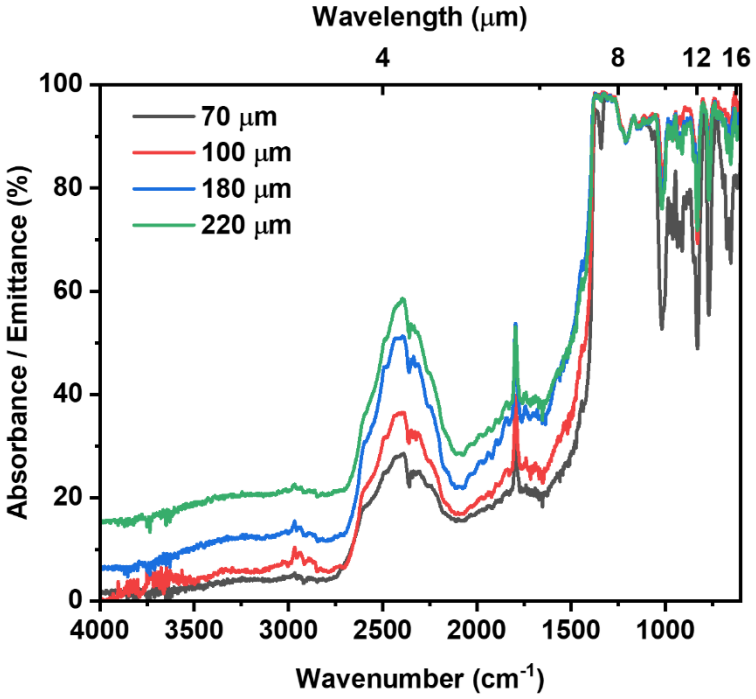

Fig. S4 IR emission depending on CYTOP thickness.

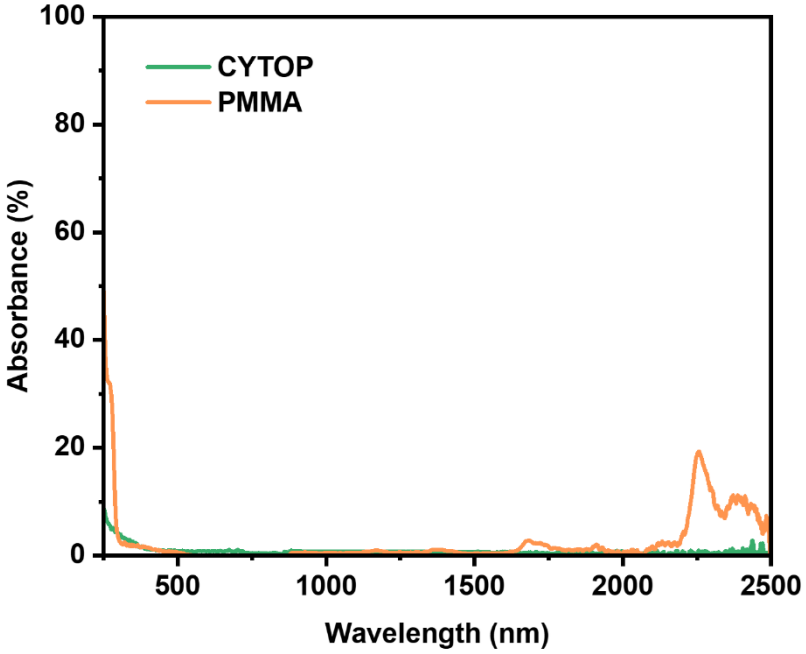

Fig. S5 UV-Vis-NIR absorption spectra of CYTOP and PMMA freestanding films.

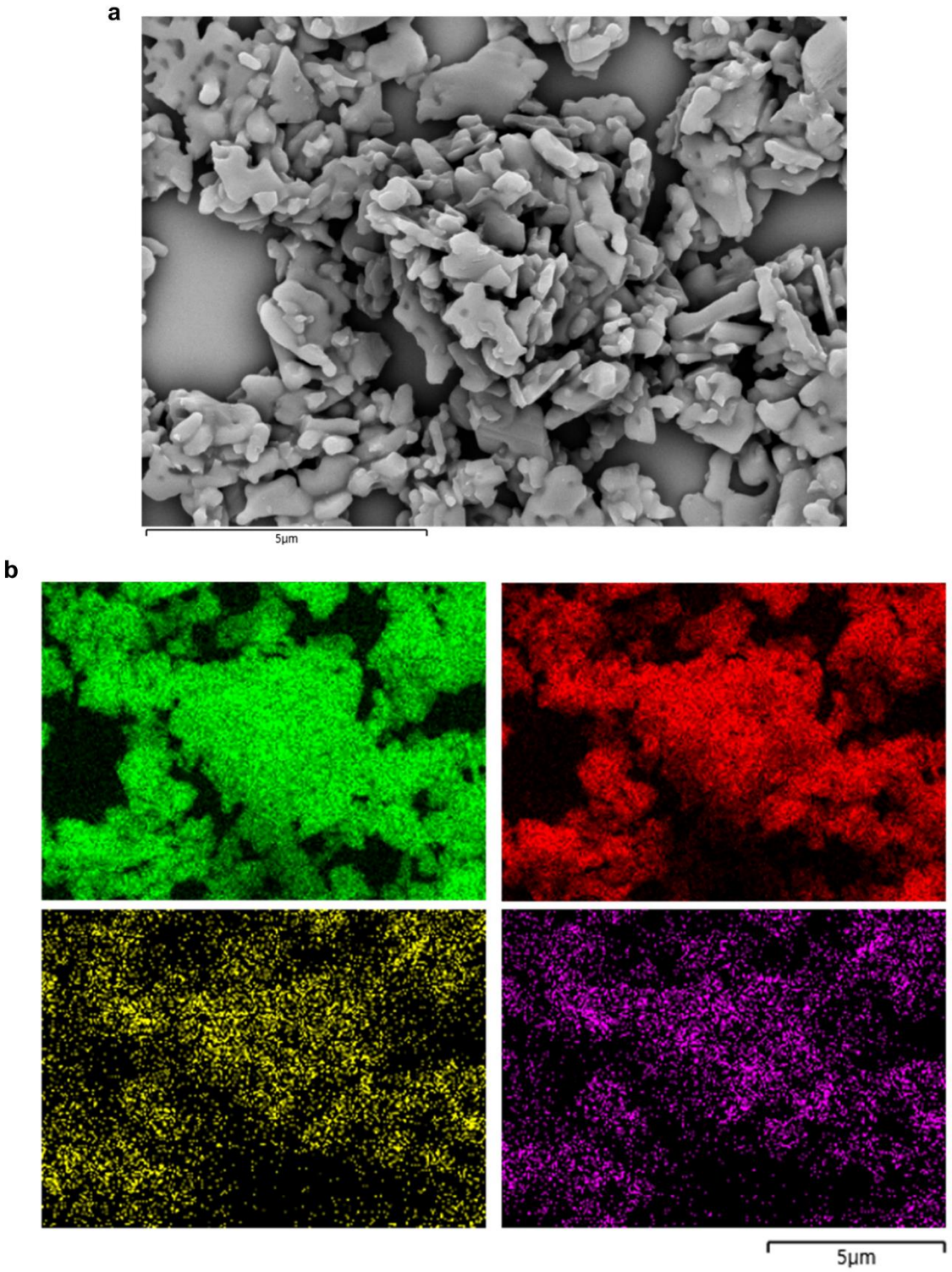

Fig. S6 a) SEM image of Al_2O_3-PFOTS nanoparticles and b) EDS elemental mapping images of Al (green), O (red), F (yellow), and C (purple).

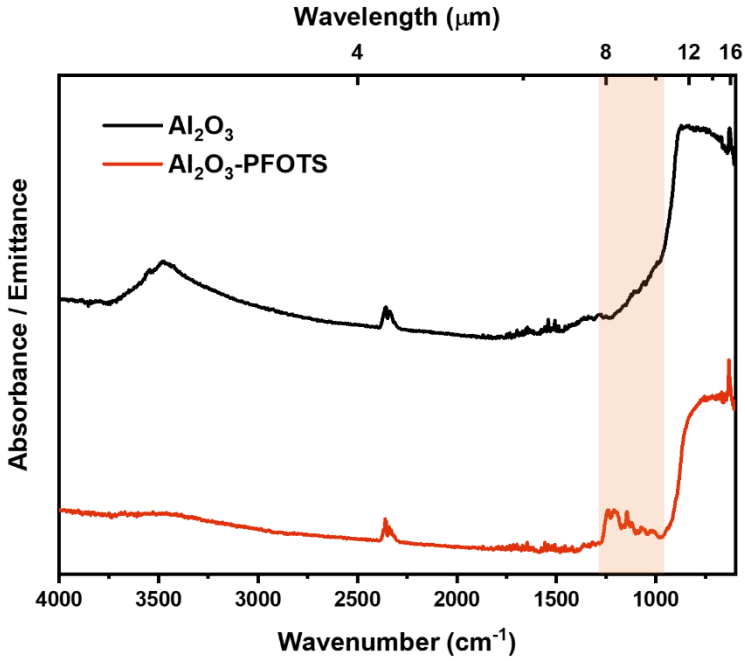

Fig. S7 FTIR spectra of Al_2O_3 (black line) and Al_2O_3-PFOTS (red line).

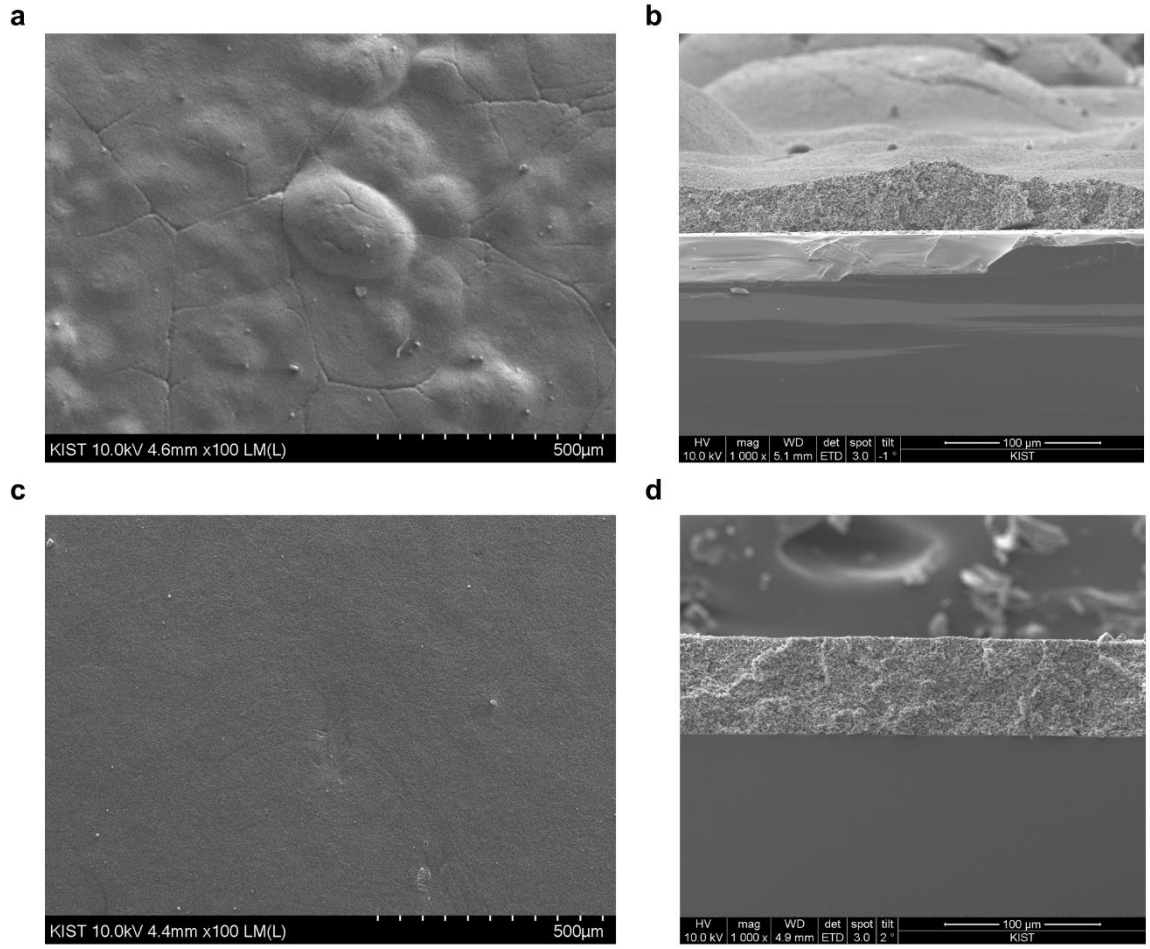

Fig. S8 SEM images of CYTOP/Al_2O_3 and CYTOP/Al_2O_3-PFOTS. a) Top view and b) cross-sectional view of CYTOP/Al_2O_3. c) Top view and d) cross-sectional view of CYTOP/Al_2O_3-PFOTS.

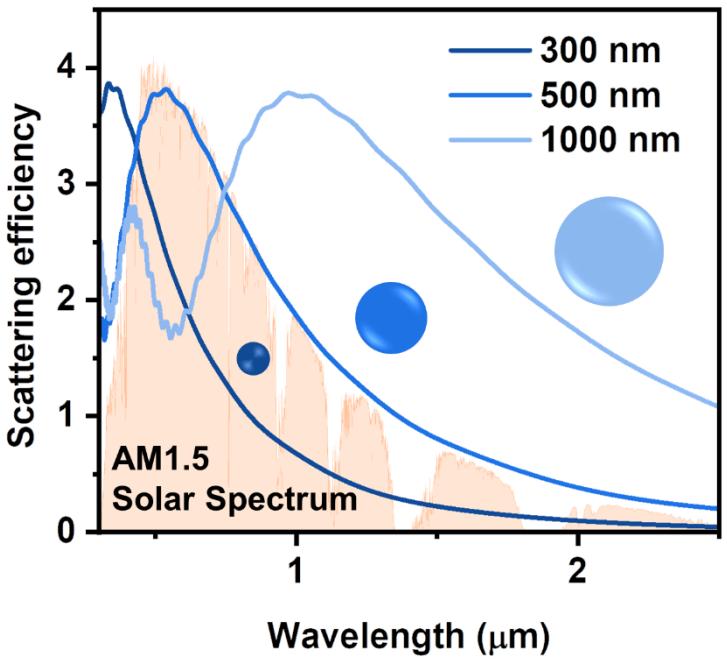

Fig. S9 Calculated Mie scattering efficiency of Al_2O_3 nanoparticles with diameters of 300, 500, 1000 nm in CYTOP matrix.

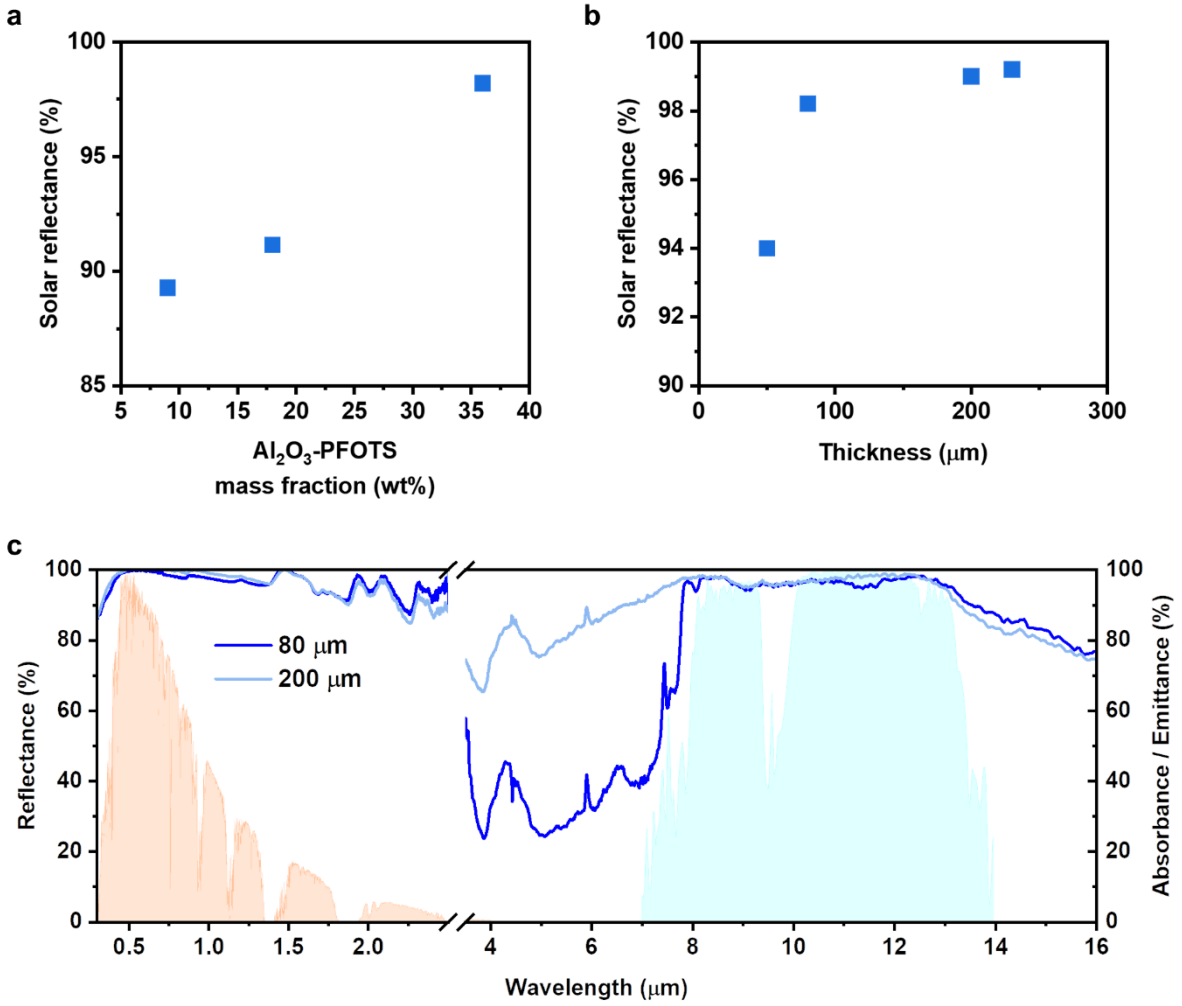

Fig. S10 a) Effect of the Al_2O_3-PFOTS nanoparticles mass fraction on the solar reflectance. b) Effect of the thickness of the CYTOP/Al_2O_3-PFOTS on its solar reflectance. c) Optical properties of CYTOP/Al_2O_3-PFOTS with thicknesses of 80 μm and 200 μm on Si substrates.

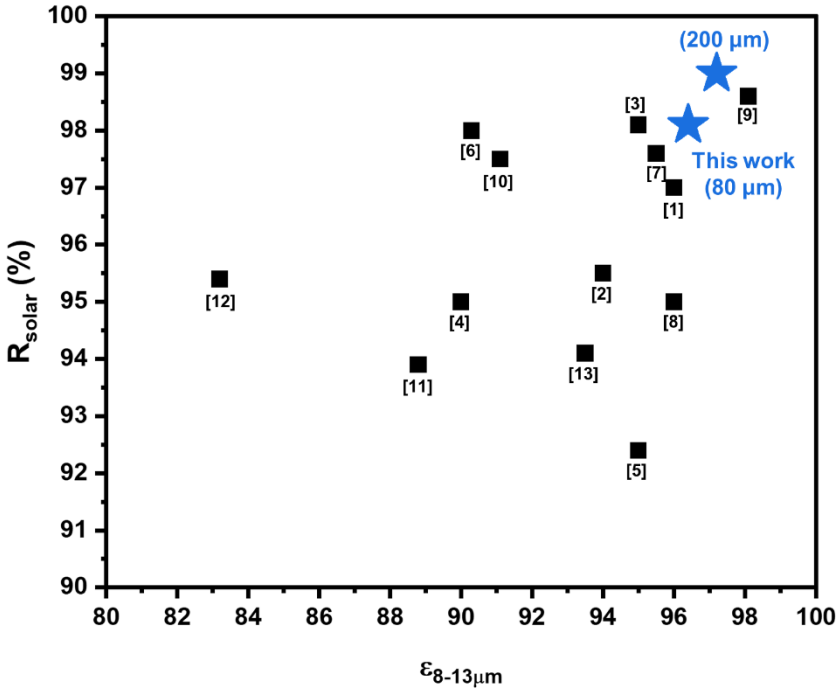

Fig. S11 Solar reflectance and IR emittance in the atmospheric window of reported emitters (black squares) compared to CYTOP/Al_2O_3-PFOTS emitters (blue stars).

Table S1 Thickness, solar reflectance, and IR emittance in the atmospheric window of reported emitters compared to CYTOP/Al_2O_3-PFOTS emitters.

Materials	**Thickness (μm)**	**Optical properties**		**Ref.**
		R_{solar} (%)	$\varepsilon_{8-13\,\mu m}$ (%)	
CYTOP/Al_2O_3-PFOTS	80	98.2	96.4	**This work**
	200	99.0	97.2	
SiO_2/PVDF/TEOS	300	97	96	[S1]
$CaCO_3$/acrylic resin	400	95.5	94	[S2]
$BaSO_4$/acrylic resin	400	98.1	95	[S3]
Al_2O_3/Silk	200	95	90	[S4]
TiO_2/PLA/PTFE	500	92.4	95	[S5]
h-BN/PDMS	1400	98	90.3	[S6]
Al_2O_3/TPU	350	97.6	95.5	[S7]
$BaSO_4$/SiO_2/PVDF	100	95	96	[S8]
$BaSO_4$/ethyl cellulose	700	98.6	98.1	[S9]
SiO_2/PVDF-HFP	250	97.5	91.1	[S10]
ZnO/HDPE	227.3	93.9	88.8	[S11]
PTFE/POM	150	95.4	83.2	[S12]
Al_2O_3/SiO_2/DPHA	250	94.1	93.5	[S13]

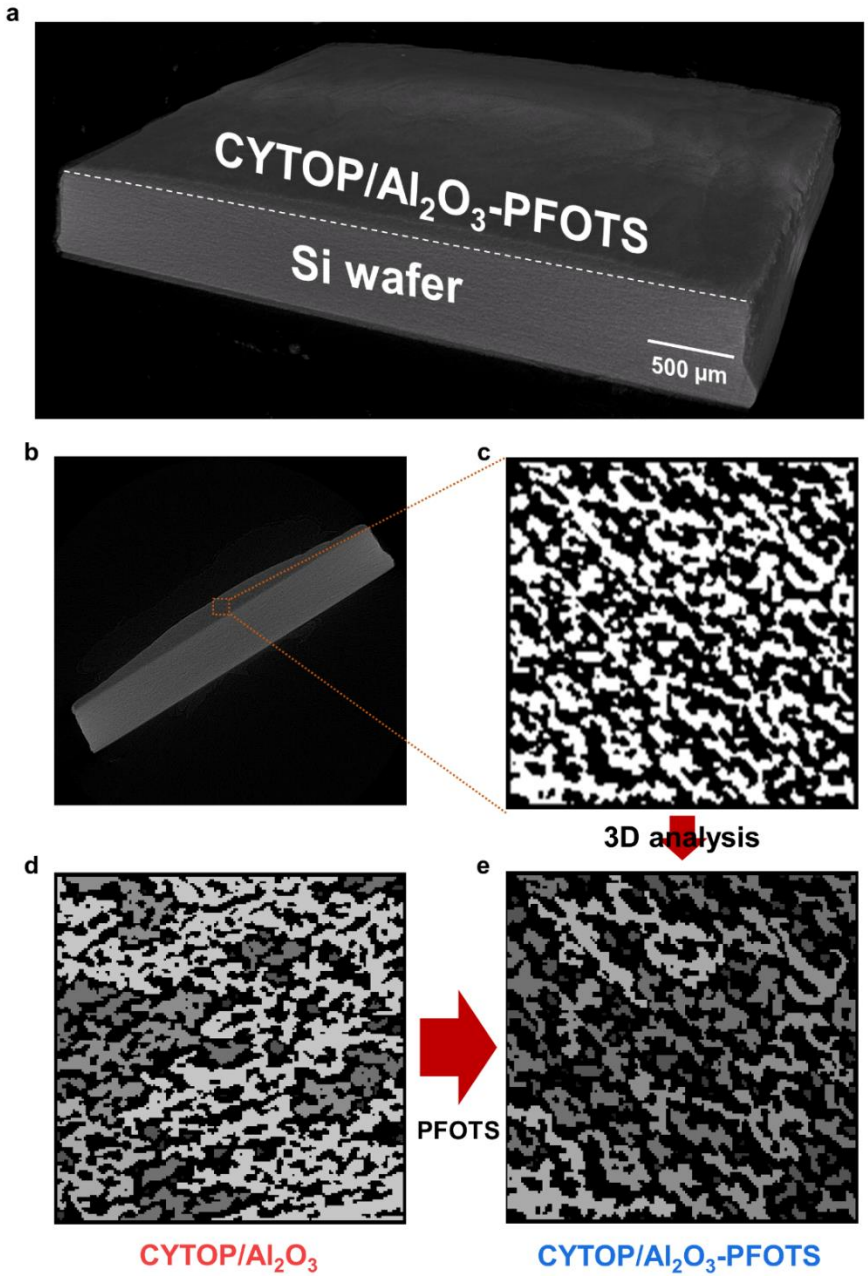

Fig. S12 a) Microstructural visualization of CYTOP/Al_2O_3-PFOTS. b) Cross-sectional image of CYTOP/Al_2O_3-PFOTS and c) binary image of the region of interest (ROI). Three-dimensional analyzed binary images of d) CYTOP/bare-Al_2O_3 (porosity: 47.1%) and e) CYTOP/Al_2O_3-PFOTS (porosity: 58.8%).

Note: In 3D analyzed binary images (Figure S12 d and e), the black areas represent air voids, while the gray regions indicate spaces filled with CYTOP/Al_2O_3(-PFOTS).

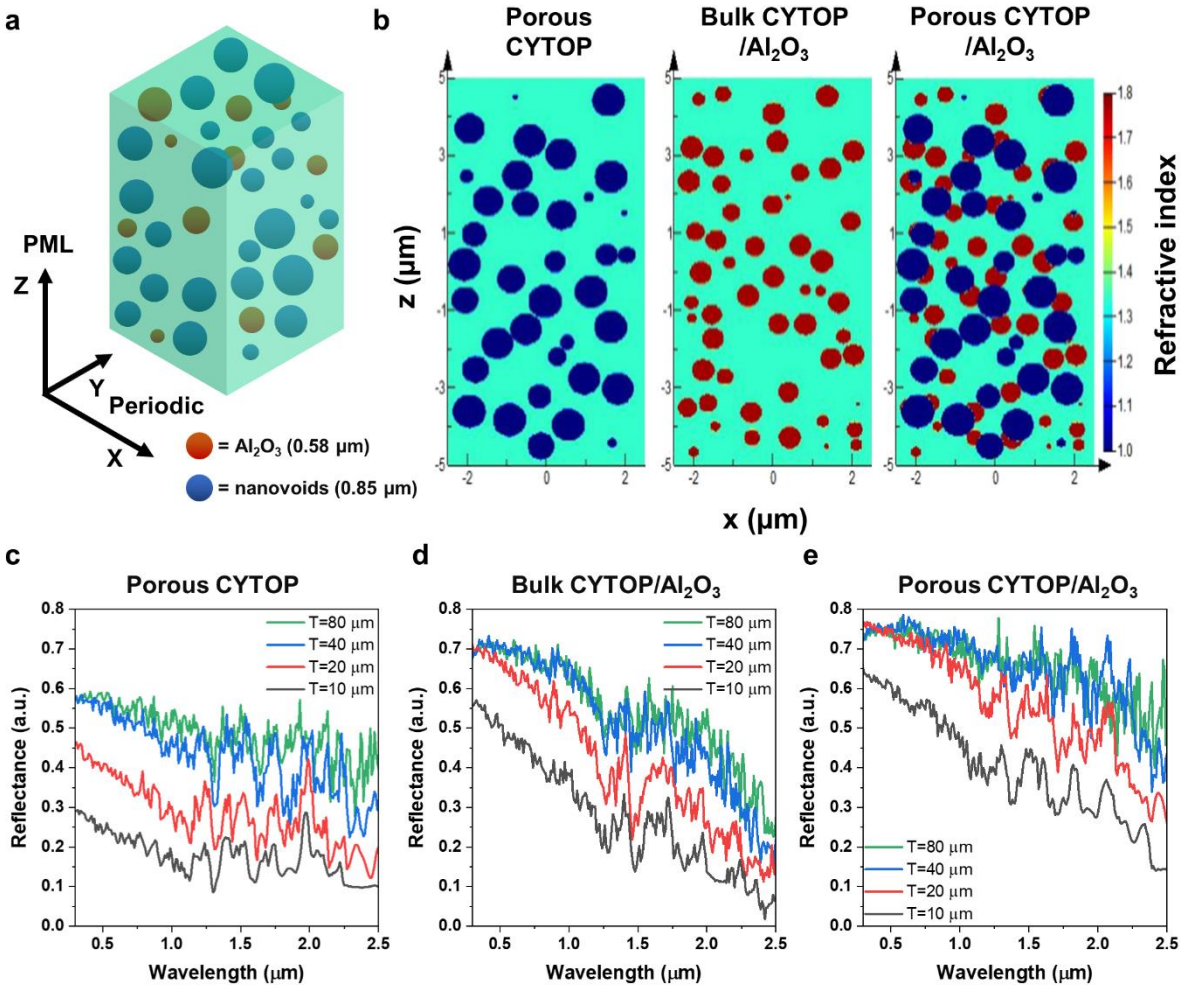

Fig. S13 a) Schematic illustration of the domain and boundary conditions for FDTD simulations. b) Cross-sectional images of the simulation domain for porous CYTOP, bulk CYTOP/Al_2O_3, and porous CYTOP/Al_2O_3. FDTD simulated reflectance spectra of c) porous CYTOP, d) bulk CYTOP/Al_2O_3, and e) porous CYTOP/Al_2O_3 with varying thicknesses.

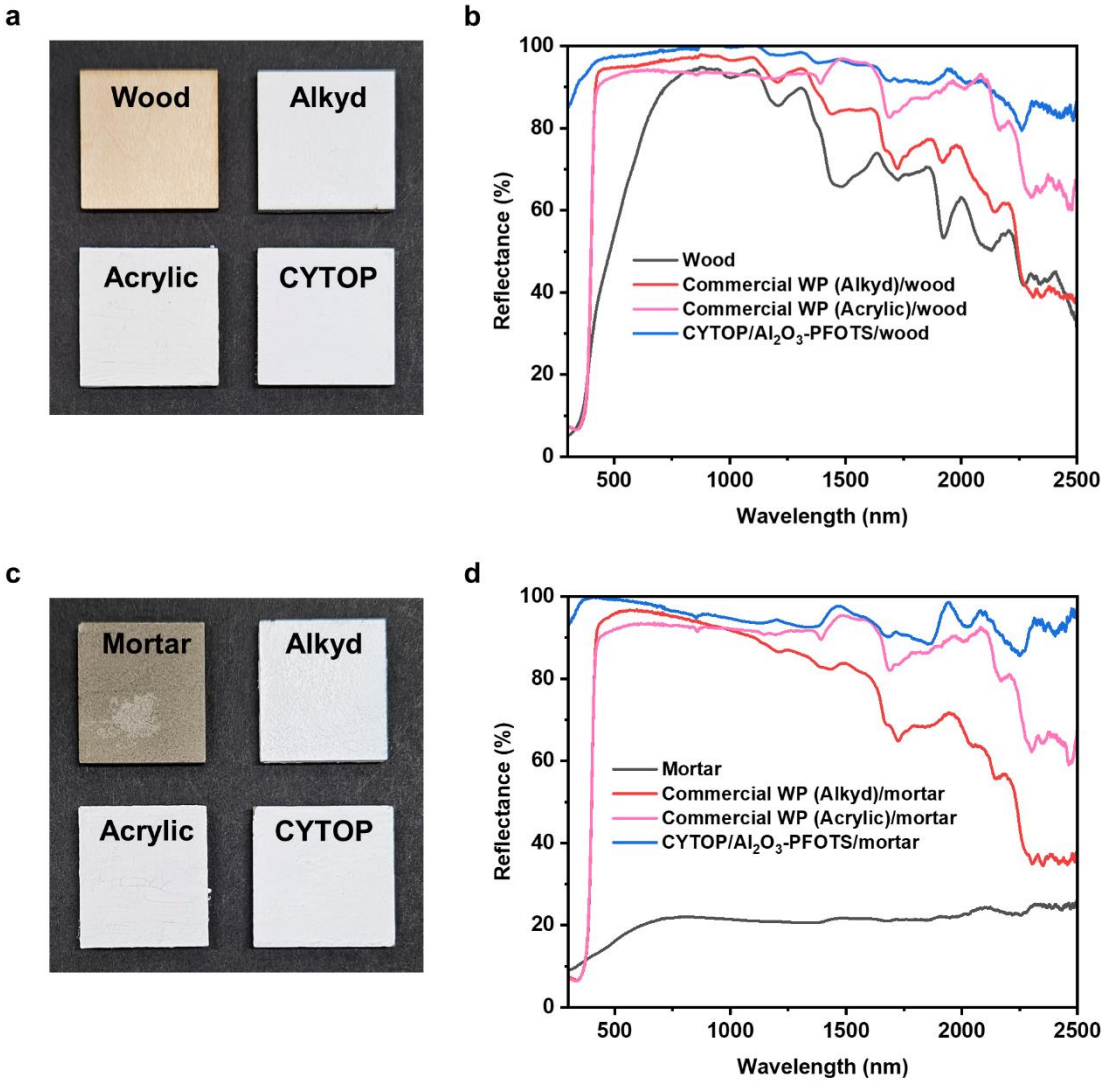

Fig. S14 Photographs of a) wood and c) mortal substrates coated with various paints: bare wood (top left), alkyd paint-coated wood (top right), acrylic paint-coated wood (bottom left), and the CYTOP/Al_2O_3-PFOTS-coated wood (bottom right). Corresponding reflectance spectra of b) the wood and d) mortar substrates.

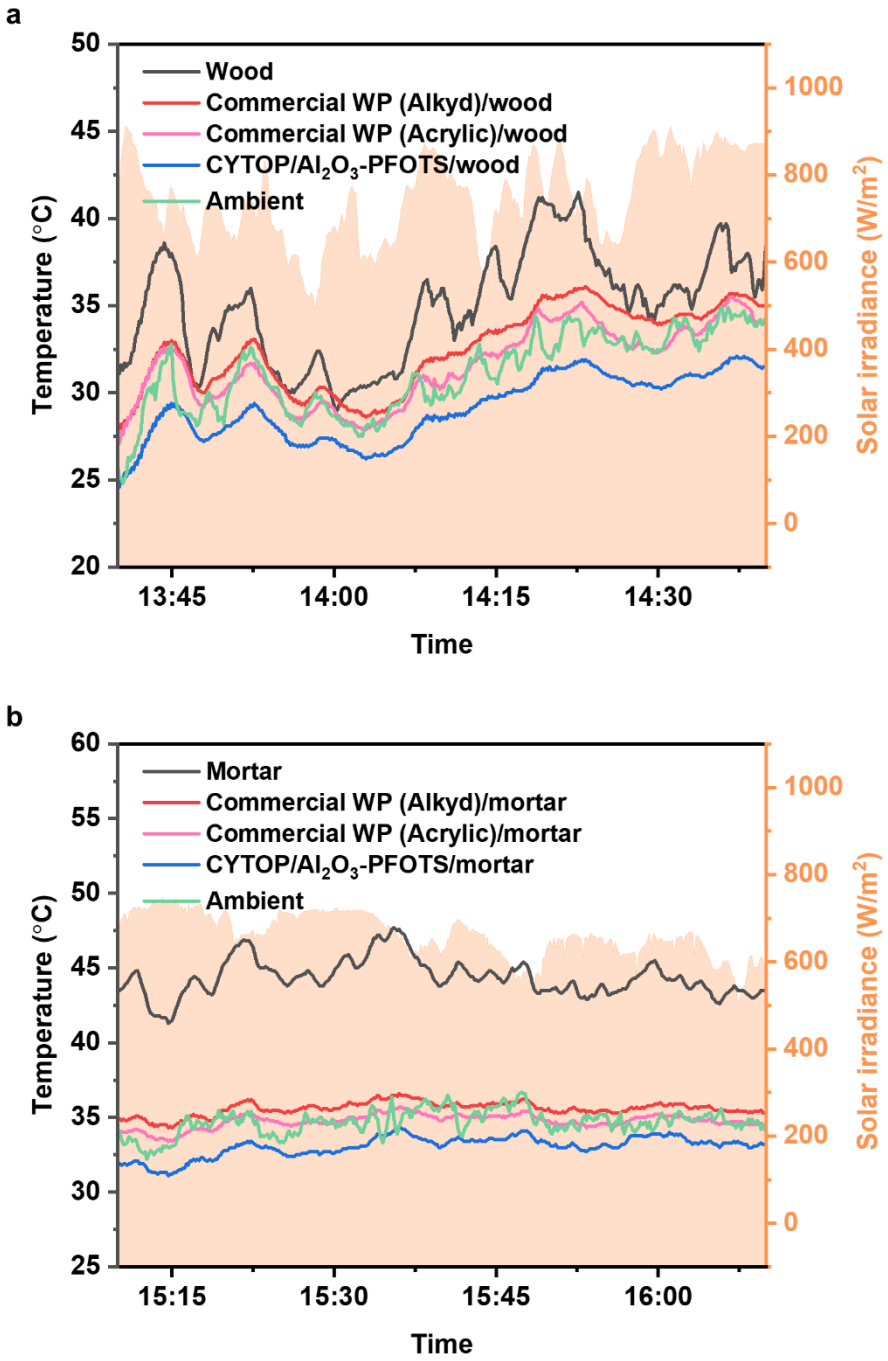

Fig. S15 Surface temperature of a) wood and b) mortar substrates coated with various paints under direct sunlight.

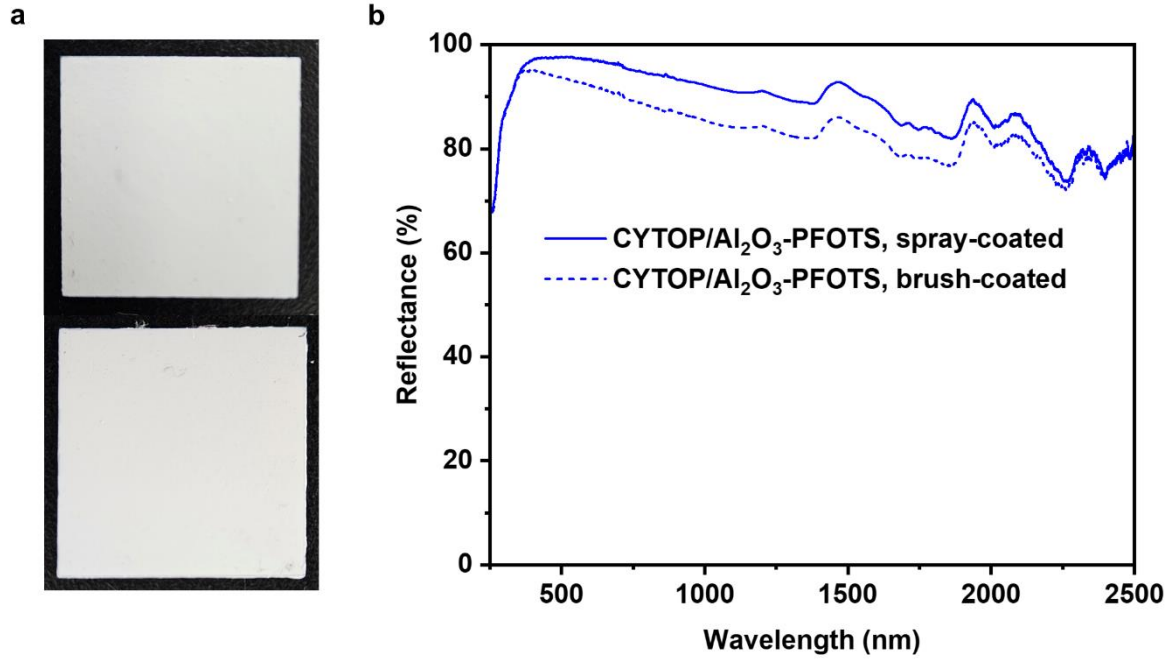

Fig. S16 a) Photograph of CYTOP/Al_2O_3-PFOTS films on Si substrates: spray-coated (top) and brush-coated (bottom). b) Reflectance spectra of CYTOP/Al_2O_3-PFOTS films using different coating methods.

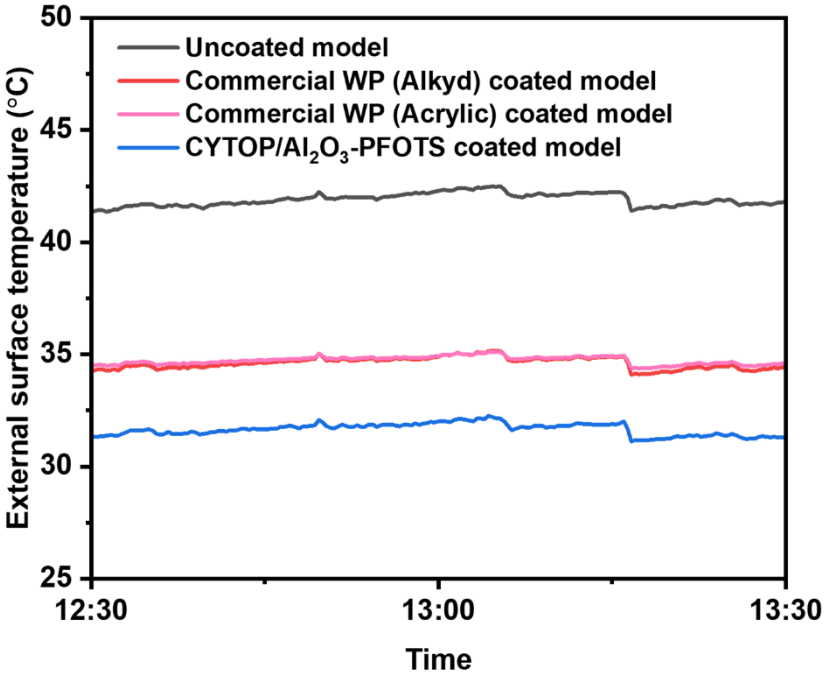

Fig. S17 External surface temperature of the miniature buildings measured using an IR camera.

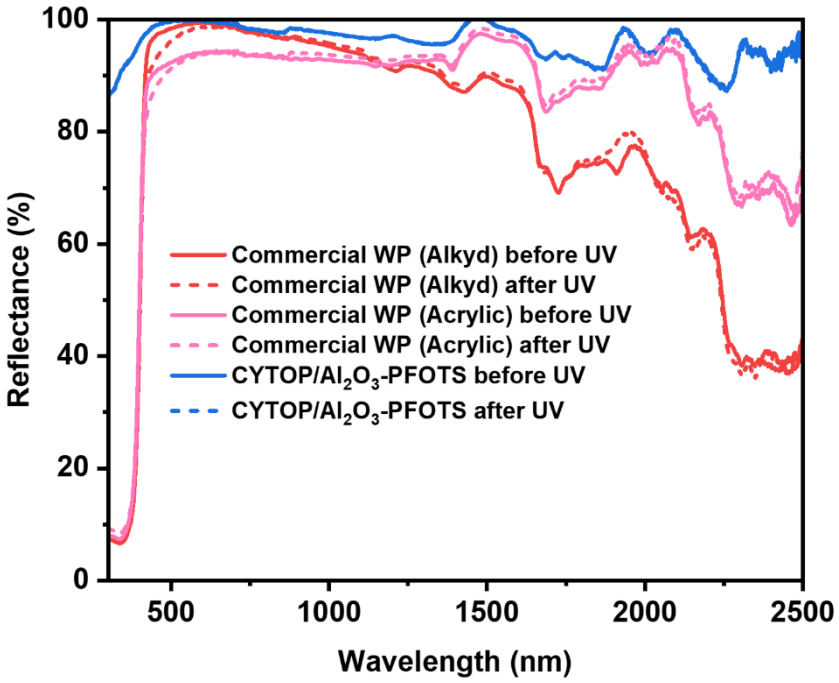

Fig. S18 Changes in the UV-Vis-NIR spectra of alkyd paint, acrylic paint and the CYTOP/Al_2O_3-PFOTS films after 720 hours of UV-A radiation (365 nm)

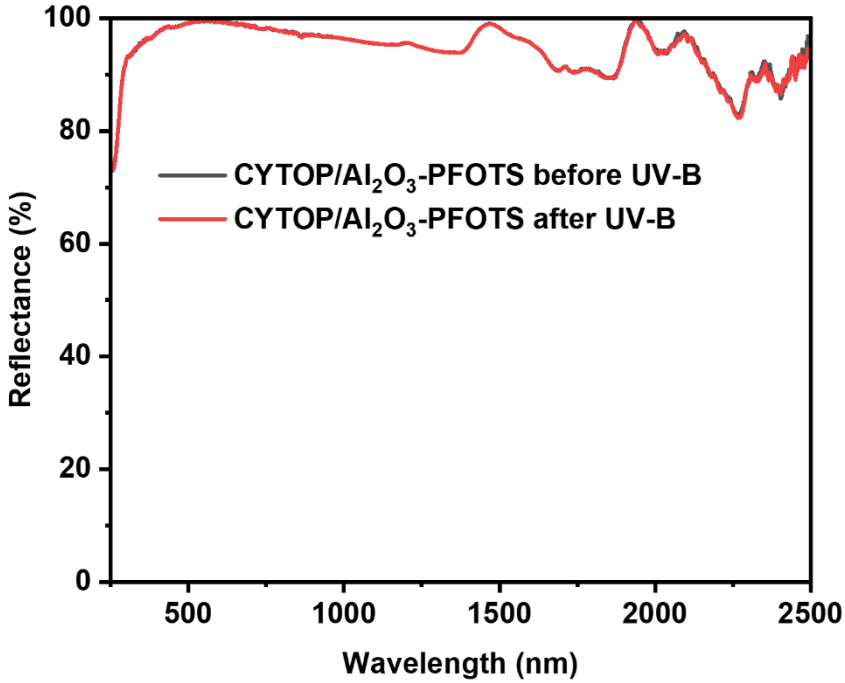

Fig. S19 Change of the UV-Vis-NIR spectrum of the CYTOP/Al_2O_3-PFOTS film after 720 hours of UV-B radiation (312 nm)

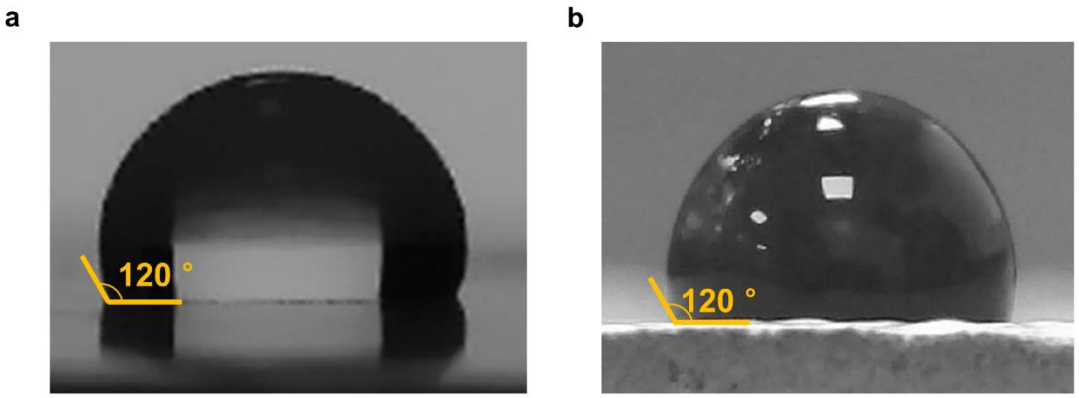

Fig. S20 (a) Water contact angle and (b) the soiling agent contact angle of the CYTOP/Al_2O_3-PFOTS surface.

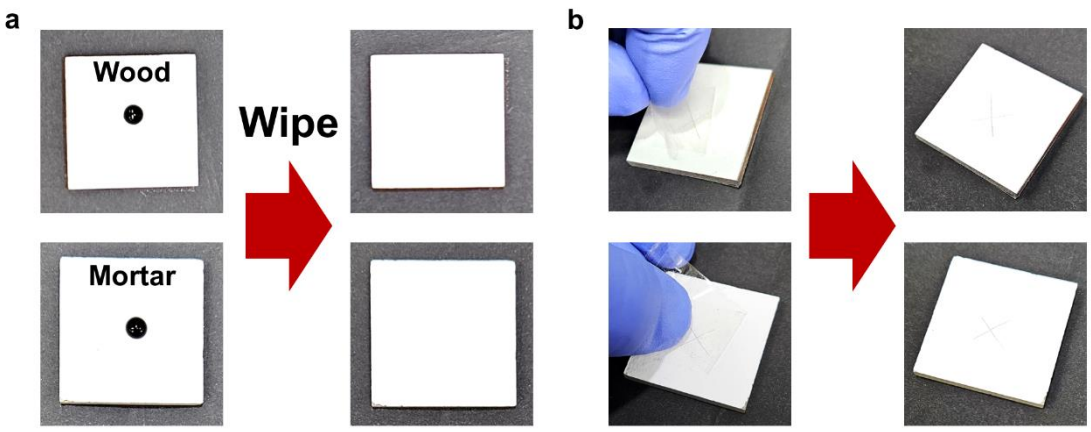

Fig. S21 (a) Anti-fouling properties and (b) adhesivity of the CYTOP/Al_2O_3-PFOTS paint on wood and mortar substrates.

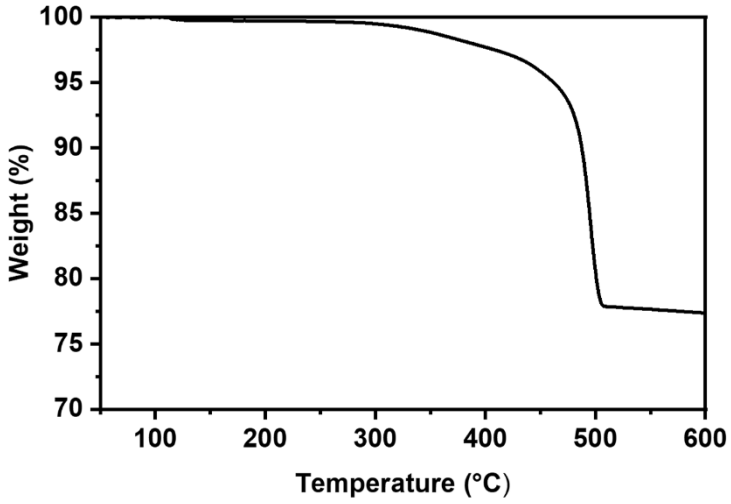

Fig. S22 TGA curve of the CYTOP/Al_2O_3-PFOTS.

Supporting References

[S1] X. Wang, X. Liu, Z. Li, H. Zhang, Z. Yang, H. Zhou, T. Fan, *Adv. Funct. Mater.* **2020**, 30, 1907562.

[S2] X. Li, J. Peoples, Z. Huang, Z. Zhao, J. Qiu, X. Ruan, *Cell Rep. Phys. Sci.* **2020**, 1, 100221.

[S3] X. Li, J. Peoples, P. Yao, X. Ruan, *ACS Appl. Mater. Interfaces* **2021**, 13, 21733.

[S4] B. Zhu, W. Li, Q. Zhang, D. Li, X. Liu, Y. Wang, N. Xu, Z. Wu, J. Li, X. Li, P. B. Catrysse, W. Xu, S. Fan, J. Zhu, *Nat. Nanotechnol.* **2021**, 16, 1342.

[S5] S. Zeng, S. Pian, M. Su, Z. Wang, M. Wu, X. Liu, M. Chen, Y. Xiang, J. Wu, M. Zhang, Q. Cen, Y. Tang, X. Zhou, Z. Huang, R. Wang, A. Tunuhe, X. Sun, Z. Xia, M. Tian, M. Chen, X. Ma, L. Yang, J. Zhou, H. Zhou, Q. Yang, X. Li, Y. Ma, G. Tao, *Science* **2021**, 373, 692.

[S6] P. Li, A. Wang, J. Fan, Q. Kang, P. Jiang, H. Bao, X. Huang, *Adv. Funct. Mater.* **2022**, 32, 2109542.

[S7] X. Liu, C. Xiao, P. Wang, M. Yan, H. Wang, P. Xie, G. Liu, H. Zhou, D. Zhang, T. Fan, *Adv. Opt. Mater.* **2021**, 9, 2101151.

[S8] Z. Cheng, H. Han, F. Wang, Y. Yan, X. Shi, H. Liang, X. Zhang, Y. Shuai, *Nano Energy* **2021**, 89, 106377.

[S9] R. Liu, Z. Zhou, X. Mo, P. Liu, B. Hu, J. Duan, J. Zhou, *ACS Appl. Mater. Interfaces* **2022**, 14, 46972.

[S10] H. Ma, L. Wang, S. Dou, H. Zhao, M. Huang, Z. Xu, X. Zhang, X. Xu, A. Zhang, H. Yue, G. Ali, C. Zhang, W. Zhou, Y. Li, Y. Zhan, C. Huang, *ACS Appl. Mater. Interfaces* **2021**, 13, 19282.

[S11] F. Peng, K. Ren, G. Zheng, K. Dai, C. Gao, C. Liu, C. Shen, *Adv. Funct. Mater.* **2024**, 34, 2400221.

[S12] X. Wu, J. Li, F. Xie, X.-E. Wu, S. Zhao, Q. Jiang, S. Zhang, B. Wang, Y. Li, D. Gao, R. Li, F. Wang, Y. Huang, Y. Zhao, Y. Zhang, W. Li, J. Zhu, R. Zhang, *Nat. Commun.* **2024**, 15, 815.

[S13] D. Chae, S. Son, H. Lim, P. H. Jung, J. Ha, H. Lee, *Mater. Today Phys.* **2021**, 18, 100389.